Probabilistic Prediction of Longitudinal Driving Behaviour for Driving Simulator Pre-Positioning

Eppink, J.M.; Kolff, M.J.C.; Venrooij, Joost ; Pool, D.M.; Mulder, Max

Publication date
2023

Document Version
Final published version

Published in
Proceedings of the 22nd driving Simulation & Virtual Reality Confrence

Probabilistic Prediction of Longitudinal Driving Behaviour for Driving Simulator Pre-Positioning

Jesse Eppink[1,2], Maurice Kolff[1,2], Joost Venrooij[1], Daan M. Pool[2], Max Mulder[2]

(1) BMW Group, Research, New Technologies, Innovations, 80788 Munich, e-mail: {Maurice.Kolff, Joost.Venrooij}@bmw.de
(2) Delft University of Technology, Faculty of Aerospace Engineering, section Control & Simulation, 2629 HS Delft, e-mail: jesseeppink@gmail.com, {m.j.c.kolff, d.m.pool, m.mulder}@tudelft.nl

Abstract - *Due to the non-deterministic nature of longitudinal human driver behaviour, motion cueing algorithms currently cannot fully utilize the workspace of driving simulators. This paper explores the possibility of using various predictor variables to predict longitudinal driving behaviour. Through the development of a logistic regression model, it is shown that a combination of the current vehicle velocity, the speed limit eight seconds ahead and the accelerator pedal deflection yields the most accurate estimate of the probabilities that drivers will accelerate or decelerate. Based on these probabilities, a driving simulator was linearly pre-positioned in combination with a classical washout algorithm. The perceived motion incongruence was subjectively evaluated by the drivers ($N = 34$), testing: (i) no pre-positioning, (ii) pre-positioning, and (iii) pre-positioning with an increased longitudinal classical washout gain enabled by the pre-positioning. Results show that the pre-positioning improves the margins with respect to the longitudinal workspace limits (better workspace management), without affecting the motion incongruence ratings. When using the increased margins to increase the longitudinal gain, however, no significant reduction in motion incongruence ratings was observed. This is likely due to the small motion space of the hexapod motion system used in the current study. However, this paper shows that longitudinal driving behaviour can be accurately predicted and can enable improved workspace utilization for driving simulators.*

Keywords: *motion cueing, behaviour prediction, pre-positioning, workspace management*

Nomenclature

MCA Motion Cueing Algorithm
CWA Classical Washout Algorithm
CPT Conditional Probability Table
AUC Area Under the Curve
ROC Receiver Operator Characteristic
TPR True Positive Rate
FPR False Positive Rate
PMI Perceived Motion Incongruence
MIR Motion Incongruence Rating
SPR Section-wise Post-hoc Rating
MPC Model-Predictive Control

1. Introduction

In driving simulation, knowledge on future vehicle states can be used by the Motion Cueing Algorithm (MCA) to pre-position the simulator (Weiss, 2006). This potentially decreases the mismatch between the reference vehicle and simulator motion, increasing the realism of the simulation (Cleij, et al., 2018) and decreasing simulator sickness. As future vehicle states depend on inherently unknown driver inputs, a *prediction* of future vehicle states is required for pre-positioning. Especially longitudinal driving behaviour is notoriously difficult to predict (Hansson and Stenbeck, 2014; Pitz, 2017), because (unlike lateral and yaw motion) longitudinal motion does not always follow the strict geometry of the road, and is thus more influenced by individual driving behaviour.

In literature, several proposed implementations for predicting longitudinal driving behaviour and simulator pre-positioning exist. In the implementation of Hansson and Stenbeck (2014), the mean vehicle accelerations when braking and accelerating were used, resulting in a reference pre-positioning offset. Pitz (2017) considered legal speed limit signs, road crossings, pedestrian crossings, and traffic lights as potential triggers for longitudinal pre-positioning. No significant improvement in objective or subjective motion cueing quality as a result of pre-positioning was reported. Recently, Kraft, He, and Rinderknecht (2022) compared several strategies, including that of Hansson and Stenbeck (2014), showing that, generally, pre-positioning results in larger allowable scaling factors of a Classical Washout Algorithm (CWA).

In literature, currently no implementation considering a driver's actual *intent* to accelerate and decelerate exists, which might be of additional use to the current implementations of vehicle velocity and the legal speed limits. Furthermore, to apply pre-positioning, it must be better understood under which conditions it provides a benefit. For small simulators, the provided benefit might be too small to be of any meaningful impact on the motion cueing quality. For large simulators, the time required to fully pre-position the simulator might be larger than the look-ahead time, such that only partial pre-positioning is possible.

This paper provides three contributions to the state-of-the-art. First, the development of a logistic re-

Figure 1: BMW's small hexapod simulator "Orange Vector".

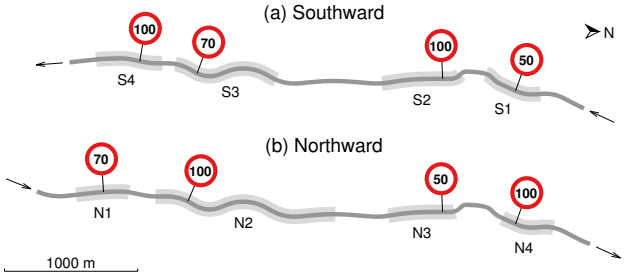

Figure 2: The southward route (a), used for fitting the prediction models, and the northward route (b), used for evaluating the prediction models and used in the experiment.

gression model for drivers' longitudinal acceleration/deceleration behaviour is described, considering speed limits, current velocity, but also the accelerator and brake pedal deflections (representing the driver's intent) as potential predictor variables. Using this logistic regression model, pre-positioning is applied to a small driving simulator in combination with a CWA. Third, the paper summarizes the results of a driver-in-the-loop experiment, in which the prediction and pre-positioning were evaluated in terms of workspace management and perceived motion incongruence.

The paper is structured as follows. Section 2 describes the development of the driver behaviour prediction module, the pre-positioning module, and the experiment set-up. The results are presented in Section 3, and are followed by the discussion in Section 4. The paper is concluded in Section 5.

2. Methods

2.1. Driver Behaviour Prediction

2.1.1. Driving Data Acquisition

First, a prediction model was developed to determine the probabilities that the driver in the loop will accelerate or decelerate. This was done by analyzing driving data from a previously performed experiment (Parduzi, Venrooij, and Marker, 2020) on a small hexapod simulator (Fig. 1) at BMW Group.

These data contain 21 southward (S) and 16 northward (N) drives on the same road through a rural area (Fig. 2). This road contains multiple speed limit signs, a small village, various curves (maximum curvature: $0.029\,\mathrm{m}^{-1}$), and hills (maximum slope: 14%). The sections in which longitudinal maneuvering takes place are denoted S1 to S4 and N1 to N4. The starting and stopping maneuvers were excluded from the analysis, as these are considered exceptions to normal continuous driving behaviour and likely require a separate approach. Participants drove a 2018 BMW 530i model with automatic transmission.

2.1.2. Model inputs

As the pre-positioning should occur below the human acceleration perception threshold, it is possible to compute the time required to pre-position the simulator. We assume this perception threshold to be $a = 0.05\,\mathrm{m/s}^2$ (Fischer, 2009). As the simulator needs half of the allowed pre-positioning distance ($d = 0.2\,\mathrm{m}$) to accelerate and half to decelerate and stop at the pre-positioning position, using $d = \frac{1}{2}at^2$ it can be derived that $t = \sqrt{2d/a} = \sqrt{2 \cdot 0.2/0.05} = 2\,\mathrm{s}$, such that $4\,\mathrm{s}$ are required to pre-position.

In order to pre-position the simulator before the acceleration or deceleration commences, it is necessary to use a larger look-ahead time t_{la} than the $4\,\mathrm{s}$ required for pre-positioning. Based on this analysis, a look-ahead time of $5\,\mathrm{s}$ is used. The maximum acceleration and deceleration between the current time and the look-ahead time, $a_{x,peak}[t \ldots t{+}5]$, was determined. To avoid the pre-positioning needlessly moving around the simulator for imperceptible acceleration improvements, only the predicted peaks larger than $0.5\,\mathrm{m/s}^2$ or smaller than $-0.5\,\mathrm{m/s}^2$ were counted as acceleration or deceleration events, respectively. This revealed that relevant accelerations occurred for 33% of the events. Deceleration was just as common (33%). In the remaining 34% of the events neither acceleration nor deceleration were present.

2.1.3. Predictor Variables

The vehicle's velocity, legal speed limits and driver control inputs were considered as potential predictor variables. Earlier analysis showed that other road environment attributes, such as the road curvature, slope, and road width are less relevant for predicting longitudinal control in this scenario (Eppink, 2020).

2.1.3.1. Vehicle velocity and legal speed limits

First, the vehicle velocity V_{veh} is considered, which was the only variable used by Hansson and Stenbeck (2014). The rationale is that at a higher velocity, deceleration becomes more likely, and vice versa. It can be expected that only considering the vehicle's current velocity is not necessarily accurate, as acceleration can still occur at high velocities (e.g., when the speed limit is increased). Similarly, deceleration can still occur at low velocities.

Therefore, the legal speed limit is considered as a predictor as well, as in Pitz (2017). This results in another predictor variable, by subtracting the legal speed limit V_{lim} from the vehicle's velocity V_{veh}. As drivers probably anticipate upcoming road signs well before reaching them, another predictor variable was defined using the speed limit further down the road instead of the speed limit at the vehicle's position. For this purpose, the speed limit that applies t_{lim} seconds in advance, $\hat{V}_{lim,t+t_{lim}}$, is used. This approach is simplified by assuming that the current vehicle velocity remains constant.

2.1.3.2. Control inputs By only considering states of the vehicle, potentially useful information directly coming from the driver is left unused. Therefore, the accelerator and brake pedal deflections (denoted δ_a and δ_b, respectively) are considered as predictor variables. Here, the rationale is that if one of the pedals is pressed, it signals the driver's intention before this becomes measurable in the vehicle motion. The pedal deflections are on a normalized range between 0 (not pressed) and 1 (fully pressed). The rate of change of pressing the accelerator deflection $\dot{\delta}_a$ was also considered as a potential predictor variable, as the act of pressing or releasing the accelerator pedal quickly likely indicates future accelerating and decelerating, respectively.

2.1.4. Model structure

2.1.4.1. Conditional probability tables Possible values for model inputs were divided into segments. The probability that a certain behaviour occurs in the near future, P, was calculated for all combinations of model input segments and assumed valid for the center of these segments, resulting in a Conditional Probability Table (CPT). The resulting CPTs were both linearly interpolated and extrapolated to calculate P for any exact set of model inputs. Each CPT contains $\prod_{i=1}^{n} m_i$ parameters, where n is the number of predictor variables and m_i is the number of segments of variable i. For simplicity, equally sized segments spanning the complete range of sample data were used. The amount of segments is a trade-off between resolution (i.e., more segments) and accuracy (i.e., more data per segment). Empirically, an m_i of 8 was chosen when one predictor variable was used. When using two predictor variables, a lower m_i of 5 was chosen, to compensate for the further segmentation of the data. CPTs were used to compare predictor variables, as they were straight-forward to use. A drawback of the CPTs is the large amount of parameters.

2.1.4.2. Logistic regression Each CPT was used to fit a logistic regression model. Here, a linear relationship is assumed between the predictor variables x_i, and the log-odds of the probability ℓ that a specific maneuver will occur in the near future (Dobson and Barnett, 2008):

$$\ell = \ln \frac{P}{1-P} = \beta_0 + \sum_{i=1}^{n} \beta_i x_i, \tag{1}$$

such that:

$$P = (1 + e^{-(\beta_0 + \Sigma_{i=1}^{n} \beta_i x_i)})^{-1}, \tag{2}$$

with the probability of the event P and the model coefficients β_i. As there are n predictor variables in each model fit, each model contains $n+1$ parameters. The `mnrfit` function in Matlab was used to determine the model coefficients.

2.1.5. Model selection

Only the southward drives were used for model fitting, whereas the northward drives were used for model evaluation. The outputs of the CPTs and logistical regression models are the probabilities that acceleration and deceleration are about to occur, i.e., $P\left(a_{x,peak}[t \ldots t+5s] > 0.5\right)$ and $P\left(a_{x,peak}[t \ldots t+5s] < -0.5\right)$, respectively. Generally, a classification threshold is selected to determine above which P-value a maneuver is predicted. Receiver Operator Characteristic (ROC) curves (Metz, 1978) were created to be able to see how the True Positive Rate (TPR) and False Positive Rate (FPR) change for various threshold values. The Area Under the Curve (AUC) was used as a performance metric independent of the selected threshold. Moreover, F_1-scores (Chinchor, 1992) were calculated for each threshold, to find the optimal classification thresholds and their corresponding scores. Both scores are in a $[0, 1]$ range, where 1 indicates perfect predictions, and 0 indicates no prediction accuracy.

Table 1: Area Under the Curve (AUC) values and highest F-scores for acceleration- and deceleration conditional probability tables for various predictor variables. The highest values are underlined and those settings were used in the further analysis.

	Acceleration		Deceleration	
Predictor variable(s)	**AUC**	**F_1**	**AUC**	**F_1**
V_{veh}	0.54	0.46	0.50	0.39
$V_{veh} - V_{lim}$	0.66	0.47	0.53	0.38
$V_{veh} - \hat{V}_{lim,t+4\text{s}}$	0.73	0.51	0.65	0.42
$V_{veh} - \hat{V}_{lim,t+8\text{s}}$	0.74	0.54	0.75	0.55
δ_a	0.81	0.60	0.71	0.53
δ_b	0.54	0.45	0.64	0.43
δ_a, δ_b	0.81	0.60	0.73	0.51
δ_a, $\dot{\delta}_a$	0.81	0.60	0.70	0.53
$V_{veh} - \hat{V}_{lim,t+8\text{s}}$, δ_a	<u>0.84</u>	<u>0.64</u>	<u>0.77</u>	0.53
$V_{veh} - \hat{V}_{lim,t+8\text{s}}$, δ_b	0.74	0.54	0.76	<u>0.57</u>

The AUCs and highest F_1-scores for the models of various combinations of predictor variables are shown in Table 1, where the best scores are underlined. It can be seen that subtracting the current speed limit from the vehicle velocity yields improved predictions compared to only considering the vehicle velocity. Even better results are obtained when using the upcoming speed limit $8\,\text{s}$ ahead. When considering only the control inputs, the accelerator pedal deflection provides AUC scores that are higher than the velocity and speed limit combinations, showing the usefulness of including this predictor variable. Adding the decelerator pedal deflection and/or the time derivative of the accelerator deflection does not improve predictions. Surprisingly, the accelerator pedal deflection predicts both acceleration and deceleration better than the brake pedal deflection. The highest prediction scores are obtained when using the vehicle's velocity w.r.t. the legal speed limit $8\,\text{s}$ ahead, combined with the accelerator pedal deflection ($V_{veh} - \hat{V}_{lim,t+8\text{s}}$, δ_a).

A graphical representation of the CPTs of this predictor variable combination is given in Fig. 3. These probabilities were interpolated to obtain finer predictions. The probabilities in the top and top right corner of the figure were initially unknown, as they represent a rather unusual combination of vehicle speed and accelerator deflection which did not occur in the training data. Model outputs in this region are obtained through linear extrapolation. It can clearly be seen that generally, a higher $V_{veh} - \hat{V}_{lim,t+8}$ decreases the chance of acceleration and increases the chance

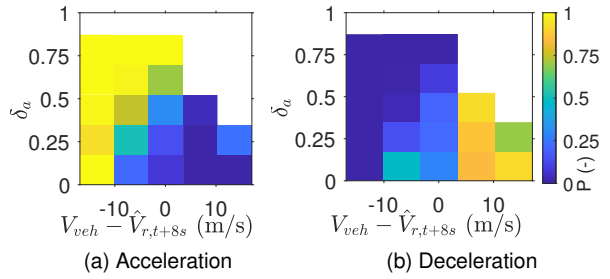

Figure 3: Conditional probability tables for acceleration/deceleration prediction with predictor variables $V_{veh} - \hat{V}_{lim,t+8s}$ and δ_a; white areas indicate a combination of both predictor variables for which no data is available.

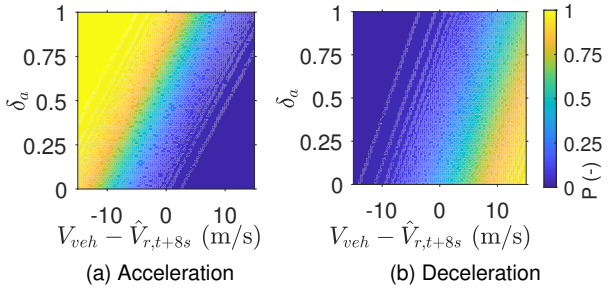

Figure 4: Logistic regression models for acceleration/deceleration prediction with predictor variables $V_{veh} - \hat{V}_{lim,t+8s}$ and δ_a.

of deceleration, whereas a higher δ_a increases the chance of acceleration and decreases the chance of deceleration.

Based on the data of the predictor variables ($V_{veh} - \hat{V}_{lim,t+8s}$, δ_a), the predicted probability (See (1)) of the acceleration is:

$$P_{acc}(t) = \left(1 + e^{-(\beta_0 + \beta_1 (V_{veh} - \hat{V}_{lim,t+8}) + \beta_2 \delta_a)}\right)^{-1}, \quad (3)$$

with $\beta_0 = -3.3$, $\beta_1 = -0.35$, and $\beta_2 = 5.6$. Similarly, for the deceleration:

$$P_{dec}(t) = 1 - \left(1 + e^{-(\beta_0 + \beta_1 (V_{veh} - \hat{V}_{lim,t+8}) + \beta_2 \delta_a)}\right)^{-1}, \quad (4)$$

with $\beta_0 = 0.62$, $\beta_1 = -0.25$, and $\beta_2 = 2.6$. These models are shown in Fig. 4, indicating that indeed the same trends as in the CPT data are present (Fig. 3). The ROC curves of both model architectures are shown in Fig. 5. The points with the highest F_1-scores are denoted with "+". No large differences are found between the two model types with regard to their ROC curves. Table 2 shows the AUC and highest F_1-scores for both model architectures. For acceleration prediction, the AUC and F_1-score are slightly better for the CPT. For deceleration prediction, the highest F_1-score is slightly better for the logistic regression model. As the logistic regression model consists of only 3 parameters, compared to the 25 parameters of the CPT, it is used throughout the remainder of this paper.

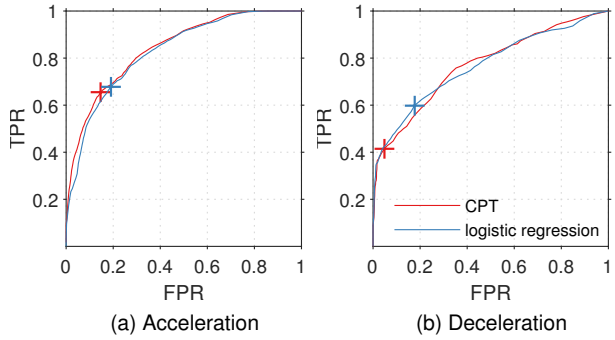

Figure 5: Receiver Operator Characteristic (ROC) curves for acceleration/deceleration prediction models with predictor variables $V_{veh} - \hat{V}_{lim,t+8}$ and δ_a. Points with the highest F_1-scores are denoted by "+".

Table 2: Area Under the Curve (AUC) and highest F-scores for acceleration- and deceleration using a Conditional Probability Table (CPT) and logistic regression with predictor variables $V_{veh} - \hat{V}_{lim,t+8}$ and δ_a.

	Acceleration		Deceleration	
Model architecture	**AUC**	**F_1**	**AUC**	**F_1**
CPT	0.84	0.64	0.77	0.53
Logistic regression	0.83	0.62	0.77	0.55

2.2. Pre-positioning

The pre-positioning module consists of two elements. First, based on the probabilities of longitudinal acceleration/deceleration from the driver behaviour prediction model, the pre-positioning is determined through the *pre-positioning logic*, see Fig. 6. Here, linear relationships between the pre-positioning position signal and th acceleration/deceleration probabilities are used:

$$p_{pp,acc}(t) = P_{acc}(t) \cdot p_{pp,min}, \quad (5a)$$

$$p_{pp,dec}(t) = P_{dec}(t) \cdot p_{pp,max}. \quad (5b)$$

The resulting pre-positioning signals are summed to obtain the total pre-positioning signal, i.e., $p_{pp,ref}(t) = p_{pp,acc}(t) + p_{pp,dec}(t)$. The pre-positioning is limited to not exceed $p_{pp,min}$ and $p_{pp,max}$: the largest allowed rear and front positions, respectively. These values must be smaller than the workspace limits, due to a possible overshoot in the pre-positioning controller, and were empirically tuned to $p_{pp,min} = -0.14\,\text{m}$ and $p_{pp,max} = 0.20\,\text{m}$.

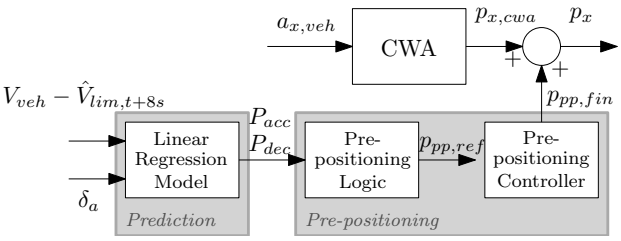

Figure 6: Merging of prediction-based pre-positioning with the Classical Washout Algorithm (CWA).

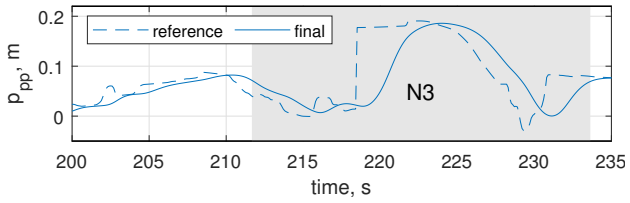

Figure 7: Linear pre-positioning for an example drive, showing the output of the pre-positioning logic (reference) and the pre-positioning controller (final).

Second, the outputs of the pre-positioning logic are limited to stay below the acceleration and jerk thresholds by the *pre-positioning controller* proposed by Fischer (2009), with thresholds of $0.05\,\mathrm{m/s^2}$ and $0.1\,\mathrm{m/s^3}$, respectively. These values have empirically been found acceptable for pre-positioning (Hansson and Stenbeck, 2014). Fig. 7 shows the reference and final signals of the pre-positioning controller, indicating the lagged response of the final position signal, as a result of the acceleration and jerk controller. This final output of the pre-positioning $p_{pp,fin}(t)$ is added to the classical washout algorithm longitudinal position output $p_{x,cwa}$ before being sent through the workspace limiting block. This limits the simulator motion and sends the final signal to the simulator.

2.3. Experiment

A driver-in-the-loop experiment was performed, similar in experiment set-up to the experiment of Parduzi, Venrooij, and Marker (2020) that was used for the model development in Subsection 2.1. Participants only drove on the Northward route, see Fig. 2(b).

2.4. Independent variables

The experiment had two independent variables: the presence of pre-positioning (active or inactive), and the longitudinal acceleration gain of the MCA ($K_x = 0.24$ or $K_x = 0.33$). Three conditions were tested. Condition C1, in which only the classical washout algorithm ($K_x = 0.24$) was tested with the pre-positioning inactive, served as the baseline. In condition C2 the pre-positioning was active, but K_x was kept as in C1, to enable testing whether adding pre-positioning improves workspace management *without* affecting motion cueing quality (Hansson and Stenbeck, 2014). In condition C3 the pre-positioning was active, whereas K_x was increased to 0.33. This increase in gain (38%) was only possible due to the presence of pre-positioning. All other MCA tuning parameters were kept constant across these experimental conditions.

2.5. Dependent variables

2.5.1. Workspace management

The evaluation of the workspace management is performed by comparing the minimum margin from the workspace edge in longitudinal direction, $d_{ws,x,min}$. The starting and stopping procedures are not included in this analysis, as the MCA and the pre-positioning module were not tuned for those. A larger margin indicates that there is more workspace available to deal with unexpected longitudinal driving behaviour or to increase the longitudinal acceleration gain of the MCA.

2.5.2. Motion Incongruence Ratings

The Perceived Motion Incongruence (PMI), defined as the deviation between the expected vehicle motion and the perceived simulator motion (Kolff, et al., 2023b), was rated by the participants. An 11-point semantic differential scale was used as Motion Incongruence Rating (MIR), where 0 indicates perfect motion and 10 indicates that the motion is highly unrealistic. Participants were asked to only rate the longitudinal PMI, as this was the only degree-of-freedom that was varied throughout the experiment. The MIR data were collected through a Section-wise Post-hoc Rating (SPR), where the PMI was rated at the end of sections N1 to N4 (see Fig. 2) separately, resulting in four SPRs per drive.

2.5.3. Hypotheses

Based on the three experimental conditions, the following hypotheses are tested:

H_1: Compared to the baseline (C1), adding pre-positioning (C2) increases the workspace management (H_{1a}), without affecting the SPRs (H_{1b}).

H_2: Compared to the baseline (C1), the combined effect of adding pre-positioning and increasing the longitudinal gain (C3) results in lower SPRs.

2.6. Participants and Procedures

Thirty-four employees of BMW Group (32 males, 2 females) took part in the experiment. They were aged between 18 and 63 years ($\mu = 37.7$ years, $\sigma = 13.4$ years). All participants were in possession of a driver's license. The yearly mileage was on average $18,161$ km ($\sigma = 9,585$ km). Participation was on a voluntary basis and participants provided informed consent. The study was approved by BMW Group and TU Delft's Human Research Ethics Committee.

Preceding the measurement phase, several training drives including all motion conditions were performed, to get participants accustomed to the simulator and the rating method. After training, the experiment started. Each participant drove each of the three conditions twice, resulting in a total of six measurement drives per participant. A 5-minute break was held after the third measurement drive. Randomized Latin square matrices were used for the conditions to balance out order effects. Participants were instructed to drive as they would do during everyday driving, without time pressure and while respecting road regulations. Traffic was only present on the opposite lane.

2.7. Rating predictions

Cleij, et al., 2018 introduced the use of continuous ratings for PMI analysis, in which drivers continuously rate the PMI through a rating interface. This method is only possible in open-loop driving (i. e., drivers are *passengers*) and results in a continuous rating signal $R(t)$. Kolff, et al. (2023b) proposed a linear model that predicts the continuous rating of the average

participant as function of mismatch signals, i.e., the difference in inertial motion (specific forces and rotational rates) between the vehicle motion $\widetilde{S}_{veh,m}(t)$ and the simulator motion $\widetilde{S}_{sim,m}(t)$, i. e., $\Delta\widetilde{S}_m(t)$, with $\widetilde{P}_m(t) = |\Delta\widetilde{S}_m(t)|$. Here, m represents the mismatch direction. The ratings can be predicted using low-pass filter transfer functions $H_m(s)$ between the measured mismatch signals $\widetilde{P}_m(t)$ (inputs) and a modeled rating signal $\tilde{R}(t)$ (output):

$$\widehat{\widetilde{R}}(j\omega) = \sum_m H_m(j\omega)\widehat{\widetilde{P}}_m(j\omega) = \sum_m K_{\widetilde{P}_m}\left(\frac{\omega_c}{j\omega+\omega_c}\right)\widehat{\widetilde{P}}_m(j\omega), \tag{6}$$

with the cut-off frequency ω_c and $K_{\widetilde{P}_m}$ the gains of the several mismatch channels. The $\widehat{(\cdot)}$-terms indicate the Fourier transforms. Kolff, et al. (2023b) showed that the continuous ratings of a classical washout algorithm as measured in that study could be largely explained when considering the mismatch channels $\widetilde{P}_{f_y}$, $\widetilde{P}_{f_x}$, and $\widetilde{P}_{\omega_z}$, with respective gains of 0.93, 0.66, and 2.77, together with $\omega_c = 0.35$ rad/s.

The usefulness of predicting continuous ratings lies in the fact that these correlate to section-wise post-hoc ratings. Kolff, et al. (2023a) found a predictive relation between $R(t)$ and SPR by considering the most incongruent point, i. e., the maximum of the continuous rating signal:

$$\text{SPR} = 1.33 \cdot \max[\widetilde{R}(t)] - 0.33 \tag{7}$$

Thus, this allows for comparing the three conditions of the experiment in an offline manner. These rating models are applied as a use-case in testing whether the subjective differences in the experimental conditions can be explained through the rating model.

3. Results

3.1. Prediction

To compare the quality of the prediction of the experiment to the preliminary data set, the AUC is determined. Across all experimental drives, the AUC was 0.80 for acceleration and 0.73 for deceleration. Both scores were lower than those calculated using the preliminary data set and presented in Table 2. When averaging over all drives, the root-mean square of the longitudinal vehicle acceleration found for the experimental data ($\mu = 0.77$ m/s^2) was 34% higher than in the preliminary data ($\mu = 0.54$ m/s^2). This indicates that participants drove more aggressively in the current experiment when compared to Parduzi, Venrooij, and Marker (2020).

As a means to analyze the prediction performance over the length of the drives, the acceleration and deceleration prediction errors ($\epsilon_{\hat{p}_{acc}}$ and $\epsilon_{\hat{p}_{dec}}$, respectively) are calculated as a function of driven distance:

$$\epsilon_{\hat{p}_{acc}}(t) = \hat{p}_{acc}(t) - y_{acc}(t) \tag{8a}$$

$$\epsilon_{\hat{p}_{dec}}(t) = \hat{p}_{dec}(t) - y_{dec}(t) \tag{8b}$$

$$y_{acc}(t) = \begin{cases} 1 & a_{x,peak}[t \cdots t+5\text{s}] \geq 0.5 \\ 0 & a_{x,peak}[t \cdots t+5\text{s}] < 0.5 \end{cases} \tag{8c}$$

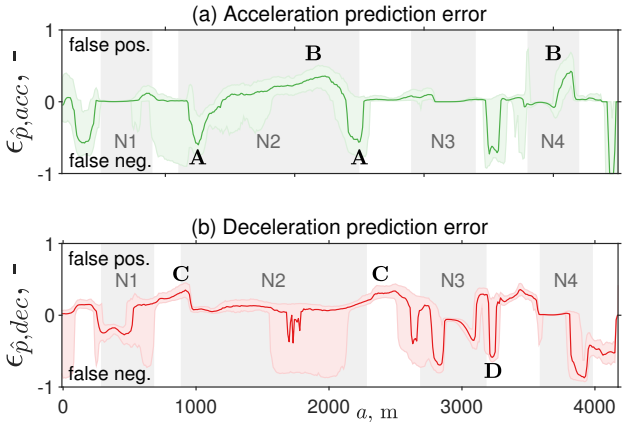

Figure 8: Medians and interquartile ranges of the acceleration and deceleration prediction errors.

$$y_{dec}(t) = \begin{cases} 1 & a_{x,peak}[t \cdots t+5\text{s}] \leq -0.5 \\ 0 & a_{x,peak}[t \cdots t+5\text{s}] > -0.5 \end{cases} \tag{8d}$$

y_{acc} and y_{dec} denote binary variables indicating whether $a_{x,peak}[t \cdots t+5\text{s}]$ exceeded the acceleration/deceleration threshold, as in Eq. (8c-d). Thus, $\epsilon_{\hat{p}_{acc}}(t)$ and $\epsilon_{\hat{p}_{dec}}(t)$ represent the error in the estimated probability of acceleration and deceleration, respectively.

Fig. 8 shows the median and interquartile range of the prediction errors against the driven distance. A positive prediction error indicates an overestimation of the probability that maneuvering will occur (i.e., false positives), and likewise, a negative prediction error indicates an underestimation (i.e., false negatives). An $\epsilon_{\hat{p}}$ of zero indicates correct predictions, which is the case for a major part of the track.

There are several points at which the prediction is incorrect, for various reasons. In the acceleration prediction error, two negative peaks are present at **A**, which are caused by differences in position on the road on which the acceleration is applied. At **B**, the accelerator deflection was increased by participants to maintain a desired velocity while driving a road with an increasing slope. As the accelerator deflection was increased merely to maintain speed, and thus not to accelerate, $\hat{p}_{acc}$ was overestimated. At **C**, many participants drove faster than the legal speed limit. When the velocity is higher than the legal speed limit, a deceleration maneuver is expected. However, since drivers maintained their velocity (or even increased it, as speeding was apparently intended) the deceleration probability was overestimated. Finally, road curvature seemed to have played a role in velocity choice of some participants, resulting in false negatives in the deceleration prediction with a relatively large spread in the behaviour, for example in N2. Furthermore, at **D** participants entered a small village, including corners. Here, drivers braked as a response to the anticipated curvature of the road. As this is not accounted for in the proposed prediction model, the deceleration probability is underestimated. Subsequently, they also accelerate again, resulting in a false negative in the acceleration prediction error.

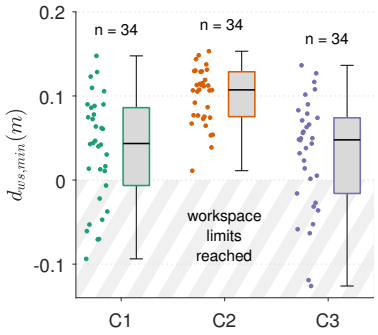

Figure 9: Workspace margin of the three conditions.

3.2. Prepositioning

3.2.1. Workspace management

The minimum workspace margin is shown in Fig. 9. The distributions were tested using a repeated measures ANOVA, revealing significant differences ($F(2, 66) = 37.8, P < 0.05$). Post-hoc testing, in which a Bonferroni correction was applied to correct for the problem of multiple comparisons, revealed that only when comparing C1 ($\mu = 0.025$ m) to C2 ($\mu = 0.084$ m), a significant increase in workspace margin was present, $t(33) = 7.38,\ P < 0.05$. The effective increase in workspace obtained using prepositioning is used to intensify cueing in C3, resulting again in a decreased workspace margin ($\mu = 0.020$ m). Negative workspace margin values indicate that workspace limits were reached. This was the case for 37% of the C1 and 34% of the C3 drives. For C2, the limits were never reached, thus showing better workspace management compared to C1 and C3.

3.2.2. Motion incongruence ratings

The SPRs are presented in Fig. 10 are calculated as the mean of the two drives for each participant. Reaching the workspace limits (Fig. 9) could result in false cues due to braking of the simulator and missing cues due to the inability to accelerate further in the direction of the workspace edge. For this reason, SPRs of sections where workspace limits were reached were omitted. The number of data points (indicated by '$n =$' in the figures) is therefore sometimes smaller than 34. Using a repeated measures ANOVA with Bonferroni correction, no significant differences were found between conditions in any of the sections. The model predictions in Fig. 10 (indicated by the cross in each graph) also show that the lack of differences in MIR could have been predicted, by calculating the predicted MIR over all drives prior to the experiment. Only the mean is shown, as the model predicts a rating of the *average* participant for each separate drive, in which individual scaling differences are not represented anymore. The estimated ratings in all conditions are lower (around 2.5) compared to the measured SPRs (between 3.5 and 6). As participants were only asked to evaluate the longitudinal PMI, it is possible that a larger gain was used by participants to rate the longitudinal motion compared to what the model accounts for, which is based on measurements of the PMI in all directions. However, the main interest lies within the differences between the three conditions, which are in line with the measured

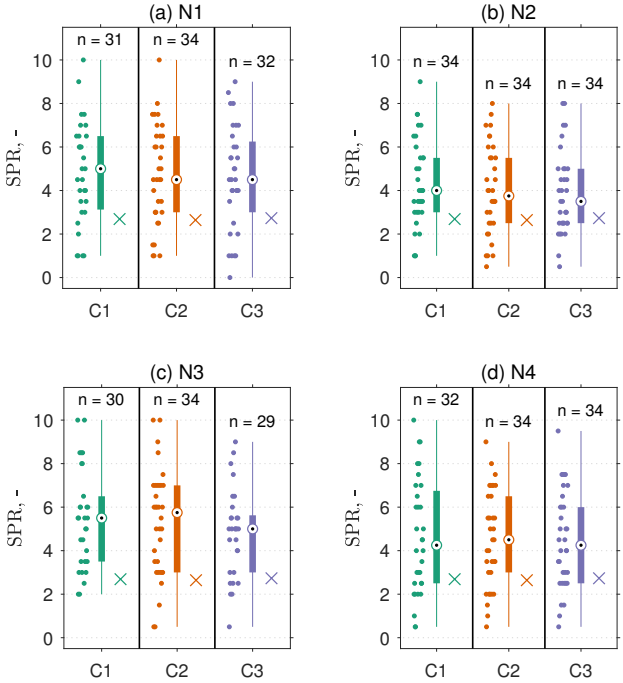

Figure 10: Section-wise Post-hoc Rating (SPR) distributions, excluding ratings of a section where workspace limits were reached. Each box plot contains a model prediction (crosses).

ratings: The model predictions confirm that no differences exist between C1 and C2, as well as that there are no differences between C1 and C3.

4. Discussion

The results of comparing the conditions C1 and C2 showed that adding pre-positioning without increasing the longitudinal acceleration gain results in larger workspace margins (i.e., better workspace management), confirming hypothesis H_{1a}. At the same time, the SPRs of all four sections showed no differences between C1 and C2, confirming H_{1b}. Increasing the longitudinal acceleration gain of the CWA from $K_x = 0.24$ (C1 and C2) to 0.33 in condition C3, however, did not result in any differences in SPR, meaning that hypothesis H_2 cannot be confirmed. Thus, these results suggest that the differences as imposed by the prepositioning were likely too small to be of any noticeable effect on the SPRs, likely caused by the limited size of the motion system.

The results of the prediction module showed that the considered predictor variables (current vehicle velocity, upcoming speed limit 8 s ahead, and the accelerator pedal deflection) accurately predict the behaviour the participants in the experiment, with the AUCs of 0.80 (acceleration) and 0.73 (deceleration), slightly lower than the values on which the prediction model was fit (0.84 for acceleration, 0.77 for deceleration). One explanation for these lower values is that even though participants were explicitly asked to drive as they would do in everyday driving, rating longitudinal motion cueing might have been an incentive to drive more aggressively. Nevertheless, as the results from the pre-analysis showed, the accelerator and brake pedal deflections provide a large contribution to the

AUC, and thus provide useful information on the prediction of longitudinal driving behaviour.

Especially this latter finding is important, because the accelerator pedal deflection is the only information that currently captures the drivers' *intent*, rather than the current state of the vehicle (vehicle velocity and speed limits). As the accelerator pedal deflection, current velocity, and the speed limit are typically available in any simulation, the presented model allows for an improvement in prediction compared to the current state-of-the-art, while allowing for implementing the prediction method in virtually any simulation without requiring more elaborate and invasive tools, such as eye trackers.

As the results showed, there are currently three limitations in the model structure. First, depending on the scenario, it is possible that the role of the slope of the road is underestimated. Here, an improvement can likely be achieved by correcting the accelerator pedal position for the slope of the road. Second, the model assumes the adherence to speed limits, which may sometimes be ignored by the drivers. Especially in German highway scenarios, where generally no legal speed limit exists, drivers can set their own maximum velocity, such that a personalized approach might be more suitable. Third, in tight curves, the velocity chosen by the driver depends more on the curvature of the road (i.e., tight corners would result in lower velocities, and vice versa), rather than the speed limit. Instead of the legal speed limit, the maximum (future) curve-driving velocity (Bosetti, Da Lio, and Saroldi, 2015) could therefore be used at instances where this velocity is lower than the legal speed limit, such as in urban scenarios.

Two additional avenues for further work are recommended. First, the AUC was used as the metric to select the best predictor variables. For the use case of pre-positioning, however, the impact of an incorrect prediction can differ depending on the situation. A false positive acceleration prediction is, for instance, worse when decelerating than when driving at a constant speed; in the first case the MCA output and the pre-positioning yield a simulator excursion in the same direction, such that the simulator limits are more likely to be reached. A model score tailored to the use-case of pre-positioning that emphasizes critical instances could help to select a more suitable prediction model. Second, for the pre-positioning it is recommended to investigate its potential benefits on larger motion systems, for which rating models as proposed by Kolff, et al. (2023b) can be used as a prediction tool. This also extends to the implementation of pre-positioning in other MCA types. Model-Predictive Control (MPC) algorithms might be more suitable for exploiting the extra knowledge on predicted states, as these can explicitly incorporate this knowledge in their optimization. For use in MPC the prediction model would need to be adapted to predict the future longitudinal acceleration signal, instead of the probabilities of braking and accelerating.

5. Conclusion

The combination of using speed limits, current velocity, and the current accelerator pedal deflection as predictor variables best predicts the drivers' acceleration and deceleration behaviour on a rural road, with an Area Under the Curve (AUC) of 0.84 and 0.77, respectively. By using this real-time prediction of acceleration and braking maneuvers, the algorithm can be used to control a pre-positioning module added to a classical washout algorithm, considerably extending the simulator workspace for representing longitudinal accelerations. In a human-in-the-loop experiment, where participants drove over the same rural road, the AUCs were 0.80 (acceleration) and 0.73 (deceleration), showing that the longitudinal driving behaviour of the participants can be successfully predicted. Compared to the baseline (C1), the addition of pre-positioning (C2) results in larger workspace margins (i.e., better workspace management). However, using these larger margins to increase the longitudinal acceleration gain (C3) yields no significant improvement in subjective motion incongruence ratings, likely caused by the too small motion system. Nevertheless, the prediction performance and the improvement in workspace management demonstrate the potential of combining information from dynamic vehicle states, driver inputs, and the road environment within the real-time simulation environment, paving the way for future prediction-based MCAs.

References

Bosetti, P., Da Lio, M., and Saroldi, A., 2015. On Curve Negotiation: From Driver Support to Automation. *IEEE Transactions on Intelligent Transportation Systems*, 16(4), pp. 2082–2093.

Chinchor, N., 1992. MUC-4 Evaluation Metrics. In: *Proceedings of the Fourth Message Understanding Conference*. McLean, VA, USA, pp. 22–29.

Cleij, D., Venrooij, J., Pretto, P., Pool, D. M., Mulder, M., and Bülthoff, H. H., 2018. Continuous Subjective Rating of Perceived Motion Incongruence During Driving Simulation. *IEEE Transactions on Human-Machine Systems*, 48(1), pp. 17–29.

Dobson, A. and Barnett, A., 2008. *An Introduction to Generalized Linear Models*. Third Edition. London, United Kingdom: Chapman & Hall/CRC.

Eppink, J., 2020. Probabilistic Maneuver Prediction for Motion Cueing in Driving Simulation. MSc Dissertation. Delft University of Technology.

Fischer, M., 2009. Motion-Cueing-Algorithmen für eine realitätsnahe Bewegungssimulation. PhD Dissertation. Technische Universität Carolo-Wilhelmina zu Braunschweig.

Hansson, P. and Stenbeck, A., 2014. Prepositioning of driving simulator motion systems. MSc Dissertation. Chalmers University of Technology.

Kolff, M., Venrooij, J., Arcidiacono, E., Pool, D. M., and Mulder, M., 2023a. Predicting Motion Incongruence Ratings in Closed- and Open-Loop Urban Driving Simulation. *IEEE Transactions on Intelligent Transportation Systems*. Under review, pre-print available.

Kolff, M., Venrooij, J., Schwienbacher, M., Pool, D. M., and Mulder, M., 2023b. Reliability and Models of Subjective Motion Incongruence Ratings in Urban Driving Simulations. *IEEE Transactions on Human-Machine Systems*. Under review, pre-print available.

Kraft, E., He, P., and Rinderknecht, S., 2022. Application of Prepositioning Strategies in a Compensational Motion Cueing Algorithm. In: *Proceedings of the Driving Simulation Conference 2022 Europe*. Strasbourg, France, pp. 127–134.

Metz, C., 1978. Basic Principles of ROC Analysis. *Seminars in Nuclear Medicine*, 8(4), pp. 283–298.

Parduzi, A., Venrooij, J., and Marker, S., 2020. The Effect of Head-Mounted Displays on the Behavioural Validity of Driving Simulators. In: *Proceedings of the Driving Simulation Conference 2020 Europe*. Antibes, France, pp. 125–132.

Pitz, J.-O., 2017. *Vorausschauender Motion-Cueing-Algorithmus für den Stuttgarter Fahrsimulator*. Wiesbaden, Germany: Springer Vieweg.

Weiss, C., 2006. Control of a Dynamic Driving Simulator: Time-Variant Motion Cueing Algorithms and Prepositioning. PhD Dissertation. Deutsches Zentrum für Luft- und Raumfahrt.